doi:10.1038/nature24642

Measurement of electrons from albedo neutron decay and neutron density in near-Earth space

Xinlin Li[1,2], Richard Selesnick[3], Quintin Schiller[4], Kun Zhang[1,2], Hong Zhao[1], Daniel N. Baker[1] & Michael A. Temerin[5]

The Galaxy is filled with cosmic-ray particles, mostly protons with kinetic energies greater than hundreds of megaelectronvolts. Around Earth, trapped energetic protons, electrons and other particles circulate at altitudes from about 500 to 40,000 kilometres in the Van Allen radiation belts. Soon after these radiation belts were discovered six decades ago, it was recognized that the main source of inner-belt protons (with kinetic energies of tens to hundreds of megaelectronvolts) is cosmic-ray albedo neutron decay (CRAND)[1]. In this process, cosmic rays that reach the upper atmosphere interact with neutral atoms to produce albedo neutrons, which, being prone to β-decay, are a possible source of geomagnetically trapped protons and electrons. These protons would retain most of the kinetic energy of the neutrons, while the electrons would have lower energies, mostly less than one megaelectronvolt. The viability of CRAND as an electron source has, however, been uncertain, because measurements have shown that the electron intensity in the inner Van Allen belt can vary greatly, while the neutron-decay rate should be almost constant[2,3]. Here we report measurements of relativistic electrons near the inner edge of the inner radiation belt. We demonstrate that the main source of these electrons is indeed CRAND, and that this process also contributes to electrons in the inner belt elsewhere. Furthermore, measurement of the intensity of electrons generated by CRAND provides an experimental determination of the neutron density in near-Earth space—2×10^{-9} per cubic centimetre—confirming theoretical estimates[4].

We obtained measurements of electron flux in the northern and southern hemispheres through the Relativistic Electron and Proton Telescope integrated little experiment (REPTile), which is on board a low-altitude satellite, the Colorado Student Space Weather Experiment (CSSWE) CubeSat[5–7]. REPTile was designed to measure the directional differential flux of protons with kinetic energies ranging from about 9 MeV to 40 MeV, and of electrons with energies from about 0.5 MeV to more than 3.8 MeV. Figure 1 shows flux data for 0.5-MeV electrons, which have been divided into ranges of L—a measurement (with units of Earth radii) of the maximum radial distance from the centre of the Earth's core magnetic field to a given magnetic field line (or, in three dimensions, a magnetic shell) that confines trapped electrons in the Van Allen belts. Electrons gyrate about a magnetic field, bounce between mirror points along a field line, and drift eastwards around a shell. If they drift around the Earth without encountering the dense atmosphere below, then they are considered stably trapped and their intensity can reach high levels. REPTile observes such stably trapped electrons in the South Atlantic Anomaly (SAA), where the magnetic-field strength is weakest and consequently shells attain their lowest altitude, as shown in Fig. 1 by the high intensity levels in the Southern Hemisphere near longitude 300° for L values greater than 1.15.

The drift orbit of an electron along an L shell has different altitudes, as illustrated in Fig. 2a. Electrons that encounter the dense atmosphere during their drift motion will lose energy to collisions and be removed from the radiation belt. However, this occurs only near the lowest point in their drift orbit—that is, in the SAA (Fig. 2b). Over the rest of their drift orbit they can be observed as 'quasi-trapped' electrons, so called because of their relatively short trapping lifetime. These electrons are seen in Fig. 1 in both hemispheres and at all L ranges in the longitude interval from about 70° to 270°; they have a lower intensity than the stably trapped electrons because they can only survive for up to one drift orbit, or about 1.5 hours. As shown in Fig. 1, the intensity increases as electrons drift eastwards towards the SAA. This uniform intensity increase with longitude implies a constant, uniformly distributed source that is able to replenish the loss that occurs in the SAA; this source is also indicated in Fig. 2b.

Also shown in Fig. 1 are local magnetic-field magnitudes at the satellite (solid lines) and at the location on the satellite's magnetic-field line at which the field magnitude is minimum (dotted lines), determined using the International Radiation Belt Environment Modeling (IRBEM)-library v.4.4 model[8]. For $L > 1.15$, stably trapped electrons in the SAA near longitude 300° are seen at the longitude of the minimum value of the local magnetic field. This minimum forms the SAA and is a consequence of the non-dipolar components of the geomagnetic field. Past measurements of inner-belt electrons ($L = 1.3$–2.5) have often been contaminated by inner-belt protons[6]. However, recent measurements from the Van Allen probes show[9] that there are few energetic protons at and below $L = 1.2$, and thus we are confident that the stably trapped fluxes shown in Fig. 1 do represent electrons. For $L < 1.15$ there is a gap in data coverage near longitude 300°. This is a result of electron-drift shells that attain minimum altitudes, in the SAA, below the satellite altitude. However, on each side of the gap the local magnetic field is seen to be equal to the field-line minimum value—that is, the satellite is at the location of the field-line minimum, a necessary consequence of the highly inclined orbit. Had any stably trapped electrons existed on these drift shells they would have been observed at the field-line minimum. Therefore, none were missed in the data gap, and the existence of the gap actually guarantees that there are no stably trapped electrons on such L shells.

The stably trapped electron flux shown in Fig. 3f (from the period 7–10 October 2012) is about three times higher than that shown in Fig. 1i (from 4–14 January 2013), but the quasi-trapped population remained the same. This dynamic variation in the population of stably trapped electrons also suggests that any possible proton contamination is unimportant to the electron measurements, because inner-belt protons are a much more stable population[9].

We have seen that the flux of stably trapped electrons peaks at the SAA for L values greater than 1.14, and that their intensity varies with L and with geomagnetic activity. Quasi-trapped electrons are seen outside the SAA and at lower L values (down to $L = 1.06$); their intensity is nearly independent of L and of geomagnetic activity. Therefore the source of the quasi-trapped electrons must be steady and uniform,

[1]Laboratory for Atmospheric and Space Physics, University of Colorado, Boulder, Colorado 80303, USA. [2]Ann and H. J. Smead Department of Aerospace Engineering Sciences, University of Colorado, Boulder, Colorado 80309, USA. [3]Space Vehicles Directorate, Air Force Research Laboratory, Kirtland AFB, New Mexico 87117, USA. [4]Heliophysics Laboratory, NASA Goddard Space Flight Center, Greenbelt, Maryland 20771, USA. [5]Space Sciences Laboratory, University of California, Berkeley, California 94720, USA.

© 2017 Macmillan Publishers Limited, part of Springer Nature. All rights reserved.

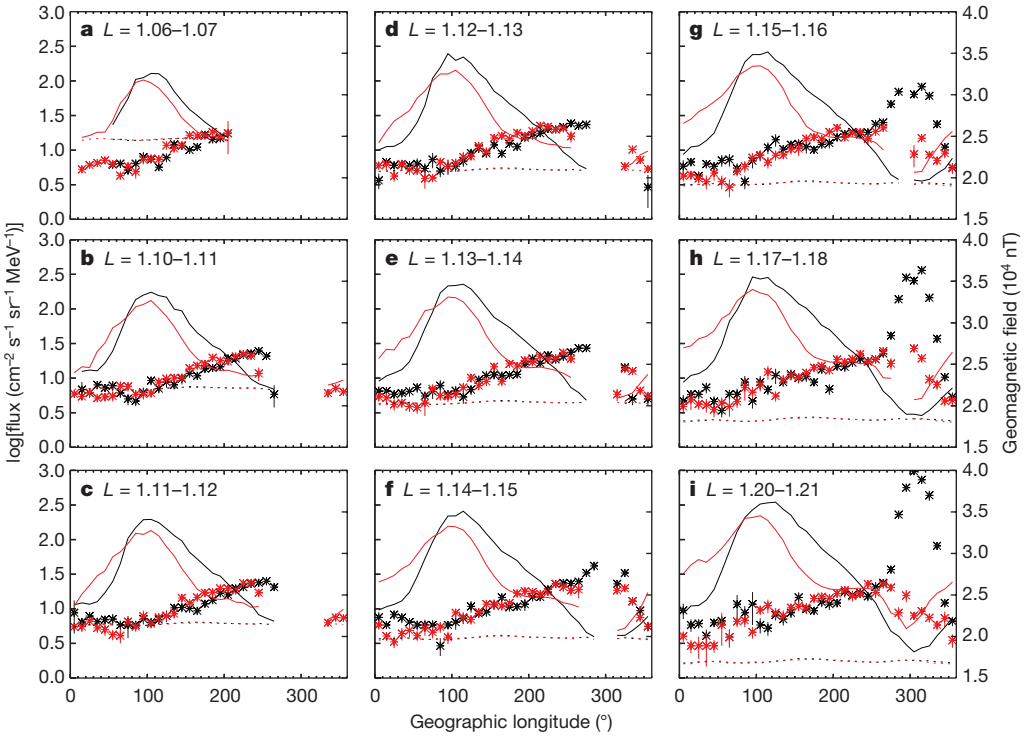

Figure 1 | Electron flux as a function of longitude in different *L* shells for the period 4–14 January 2013. a–i, Measurements of 0.5-MeV electrons at different *L* values in the southern (black asterisks) and northern (red asterisks) hemispheres, obtained by the REPTile experiment, part of CSSWE[5–7]. CSSWE, a student-built experiment involving more than 65 graduate and undergraduate students, is a three-unit (each unit being 10 cm × 10 cm × 10 cm) CubeSat mission funded by the NSF, and was launched into a low-altitude (480–790 km), highly inclined (65°) orbit on 13 September 2012 as a secondary payload under NASA's Educational Launch of Nanosatellites Program. Data are binned for different *L* shells (0.01 increments) and longitudes (10° increments beginning at 0; *x* axis) and averaged over the period 4–14 January 2013. Before averaging, data points that were ten times larger or smaller than the average of the two neighbouring points were filtered out; this accounts for 1.9% of the total data points for this time period. The error bars are in units of flux per square root of *N* (where *N* is the number of data points within a given longitude and *L* bin, and varies from 1 to 105); the error bars are visible only when *N* is small. The population of trapped electrons is seen at $L > 1.14$, below which only the quasi-trapped population exists. The local magnetic field (solid black and red lines), based on the IGRF-11 model at the CSSWE positions, is also binned according to *L* and longitude and averaged over the same time period. The dotted line shows the minimum magnetic field (at the magnetic equator) along the field line on which CSSWE is located (black for southern and red for northern latitudes), calculated using IRBEM-library v.4.4 (ref. 8) and averaged over the same time period.

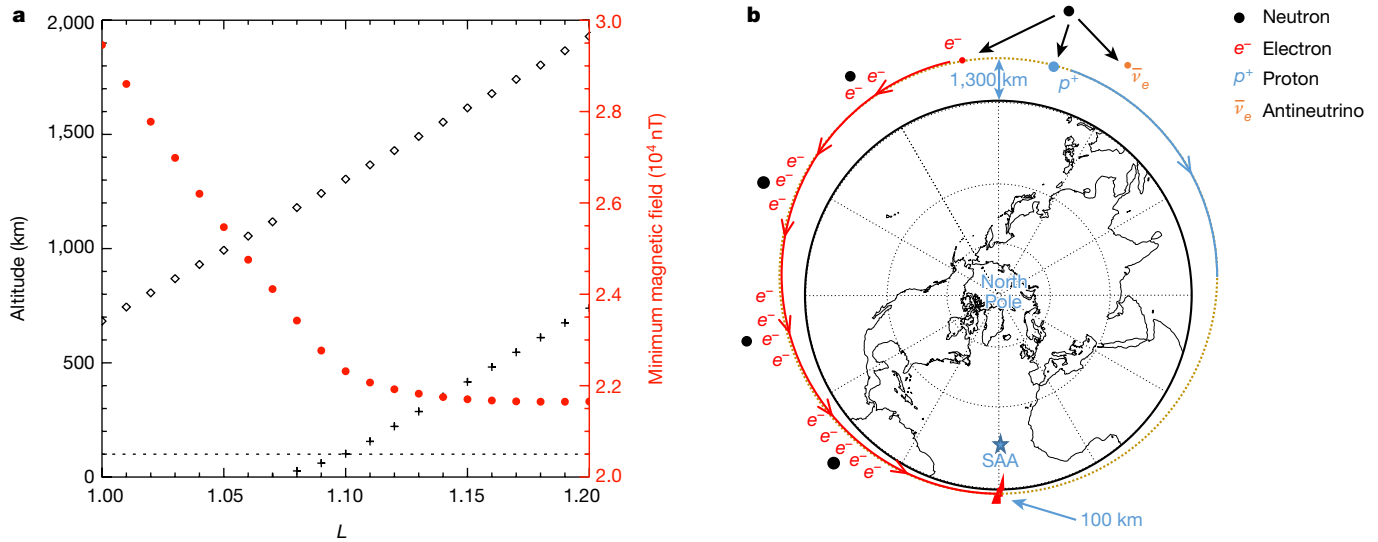

Figure 2 | Dependence of an electron's drift path on its altitude and *L* shell. a, Black symbols show the minimum altitudes (plus symbols) and maximum altitudes (diamonds) of equatorially mirroring electrons as a function of their *L* shell. The red filled circles represent the minimum magnetic-field magnitudes around the Earth at an altitude of 100 km for the given *L* shells; these minima occur in the SAA, at about 300° longitude, because the Earth's magnetic field is weakest there. All altitudes and magnetic-field minima were calculated using IRBEM-lib v.4.4 (ref. 8). The horizontal dashed line at 100 km represents the altitude at which electrons are regarded as lost to collisions with the atmosphere. **b**, An illustration of how electrons (e^-) generated by CRAND at low altitudes (lower than 1,300 km) near the equator will accumulate as they drift eastwards and precipitate in the SAA. Such electrons are referred to as quasi-trapped, because they will not complete their drift path around the Earth.

© 2017 Macmillan Publishers Limited, part of Springer Nature. All rights reserved.

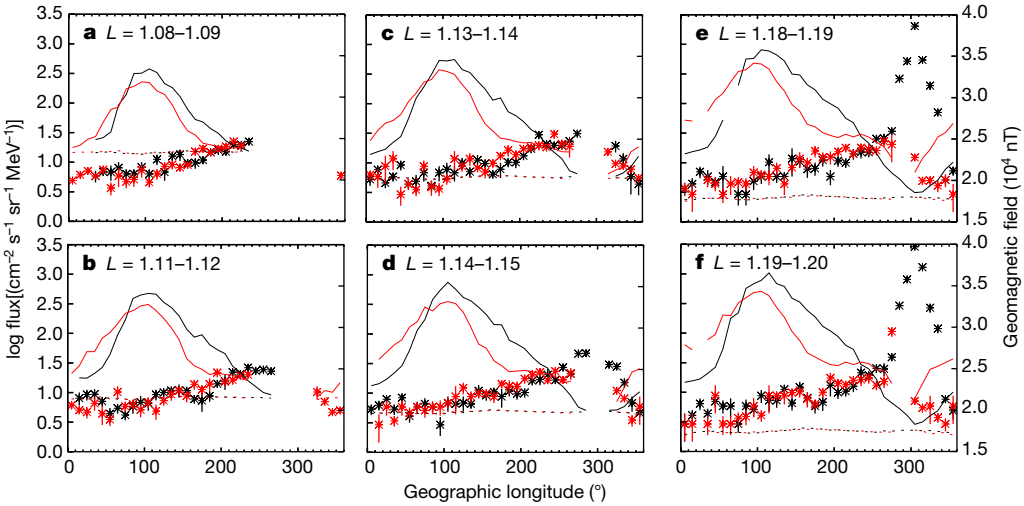

Figure 3 | Electron flux as a function of longitude in different *L* shells for the period 7–10 October 2012. a–f, Measurements of 0.5-MeV electrons at different *L* values in the southern (black asterisks) and northern (red asterisks) hemispheres. Black and red lines show the local magnetic fields for the southern and northern hemispheres; the dotted line shows the minimum magnetic field along the field line on which CSSWE is located. This time period was more geomagnetically active (the disturbance storm-time index reached −109 nT) than that shown in Fig. 1 (where the index stayed above −30nT). The trapped electron flux at $L = 1.2$ was a factor of three higher than in Fig. 1, while the quasi-trapped electron flux remained about the same. Before averaging, data points ten times larger or smaller than the average of the two neighbouring points were filtered out, amounting to 2.6% of the total data. *N* varies from 1 to 52 for this time period.

consistent with CRAND. However, we must also consider other possible interpretations.

REPTile's measurements do not distinguish electrons by arrival direction (within REPTile's field of view of about 52°). Electrons with different pitch angles (the angle between their velocity vector and the magnetic field) can have different *L* values even at the same location; this is called 'drift-shell splitting'[10,11]. If, as a result, some *L* values assigned to the data were in error, then perhaps quasi- and stably trapped electrons are actually present in the same *L* range, and the stably trapped electrons could be the source of the quasi-trapped electrons through scattering. However, using the publicly available International Geomagnetic Reference Field (IGRF) model, we found the largest *L* variation due to drift-shell splitting to be about 0.02 (Fig. 4), ruling out this possibility. Another source of error in *L* could be a large-scale electric field, which can distort drift shells and change *L* values by an energy-dependent factor. However, estimates of this effect are also too small (the change in *L* is about 0.01)[12,13].

Accepting that quasi-trapped electrons do exist in lower *L* shells while stably trapped electrons do not, another possibility is that electrons are transported inwards from the stably trapped population. They would become quasi-trapped simply because stable trapping is impossible in lower *L* shells. However, rapid transport would be needed and this would require strong geomagnetic activity to generate the required field perturbations, but geomagnetic activity is intermittent by nature and could not drive the required steady inward transport[14–17]. Even if it could, the stably trapped electron source is variable and thus cannot provide a steady source. Therefore, the requirement for a steady source of quasi-trapped electrons, at *L* values below those at which stably trapped electrons are present, seems to be consistent only with CRAND.

Moreover, given that the quasi-trapped electron intensity in higher *L* shells is essentially the same as the intensity in lower *L* shells, its source must also mainly be CRAND rather than scattering from the stably trapped population[18,19]. In addition, CRAND must also be contributing to the stably trapped electron intensity. It can be seen from Fig. 1 that the quasi-trapped differential flux reaches about 25 electrons cm^{-2} s^{-1} sr^{-1} MeV^{-1} at 0.5 MeV in less than a drift period of about 1.5 hours. At this rate, in 30 days the intensity from CRAND would be about 10^3 electrons cm^{-2} s^{-1} sr^{-1} MeV^{-1}, which is approximately the stably trapped level observed at $L = 1.2$ during quiet magnetic conditions. However, other factors affect the stably trapped intensity during active magnetic conditions, as shown by its variability. With this new understanding, we will need to re-evaluate the pitch-angle scattering and decay of the inner radiation belt electrons[18,19].

We have compared our measurements with those from other satellites with similar orbits, such as DEMETER[20], and confirmed our

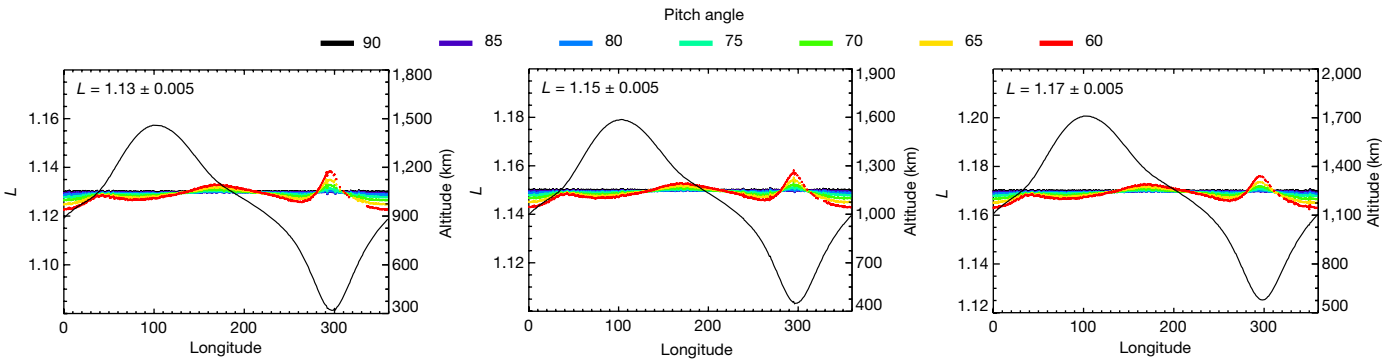

Figure 4 | Calculations showing the negligent effect of drift-shell splitting. In model calculations, electrons with different equatorial pitch angles are placed at the magnetic equator at different longitudes (every 0.5°), for three *L* bins. Their variation in *L* is the magnitude of drift-shell splitting. The black solid curves show the corresponding altitudes of the given *L* bin at different longitudes at the magnetic equator.

© 2017 Macmillan Publishers Limited, part of Springer Nature. All rights reserved.

findings (Extended Data Fig. 1). The quasi-trapped electron intensity at a fixed energy in the inner belt does not vary substantially over extended intervals (of years), as is expected from a steady CRAND source. We confirmed CRAND as a source of quasi-trapped electrons by studying REPTile's measurements as a function of longitude at very low L values, where we see that the quasi-trapped population remains steady even without any stably trapped population (Figs 1a–e and 3a–c).

CRAND electrons are produced mostly from low-energy and thermal albedo neutrons, which have a well known β-decay energy spectrum[21] that results in electrons with an upper energy limit of 782 keV (this is the mass energy difference between the neutron and the proton plus electron, $(m_n - m_p - m_e)c^2$, where m_n, m_p and m_e are the masses of a neutron, proton and electron, and c is the speed of light). The quasi-trapped electron intensity can therefore provide an estimate of the near-Earth neutron density, which has not been measured well directly because of contamination by neutrons produced locally by cosmic-ray particles or by trapped inner-belt protons striking the spacecraft that bears the detector.

Given that the mean lifetime of neutrons is also well known, the rate at which the quasi-trapped electron flux increases with longitude gives us the neutron density:

$$n = 4\pi\left(\frac{T_n}{fT_d}\right)\frac{J}{v\varphi} \quad (1)$$

where $T_n = 887$ s is the mean neutron lifetime; $T_d = 5{,}642$ s is the drift period for a 0.5-MeV electron that is bouncing between mirror points at the magnetic equator at $L = 1.2$; $f \approx 0.8$ is the fraction of a full drift completed (from the east of the SAA to the west of the SAA); $v = 2.6 \times 10^{10}$ cm s^{-1} is the electron speed; and φ is the normalized β-decay spectrum, or the probability distribution for the production of electron kinetic energy from neutron decay in the rest frame of the neutron (1.2 MeV^{-1} for an electron energy of 0.5 MeV)[21]. On the basis of Fig. 1, the highest flux of quasi-trapped electrons (J) for 0.5-MeV electrons is 25 electrons cm^{-2} s^{-1} sr^{-1} MeV^{-1}, and equation (1) gives $n = 2 \times 10^{-9}$ cm^{-3}, which is comparable to the theoretically estimated density of neutrons in near-Earth space (see figure 11 of ref. 4, which gives the electron-production rate from neutron decay; multiplying by the lifetime of 887 s gives the neutron density). This experimentally determined thermal neutron density will help us to quantify the source, the pitch-angle scattering, and the decay rate of the inner-belt electrons.

Neutron measurements have been made inside and outside the International Space Station (ISS; H. Matsumoto, personal communication). Neutron fluxes measured outside the ISS are proportional to the distance from the ISS to the SAA, suggesting that locally produced neutrons from trapped inner-belt protons striking the station are dominating the measurements. Our determination of the albedo neutron density, however, is not contaminated by locally produced neutrons, because we measured neutron-produced electrons along the whole electron-drift path.

Online Content Methods, along with any additional Extended Data display items and Source Data, are available in the online version of the paper; references unique to these sections appear only in the online paper.

Received 22 July; accepted 4 October 2017.
Published online 13 December 2017.

1. Singer, S. F. "Radiation belt" and trapped cosmic-ray albedo. *Phys. Rev. Lett.* **1,** 171 (1958).
2. Kellogg, P. J. Van Allen radiation of solar origin. *Nature* **183,** 1295–1297 (1959).
3. Lenchek, A. M., Singer, S. F. & Wentworth, R. C. Geomagnetically trapped electrons from cosmic ray albedo neutrons. *J. Geophys. Res.* **66,** 4027–4046 (1961).
4. Hess, W. N., Canfield, E. H. & Lingenfelter, R. E. Cosmic-ray neutron demography. *Geophys. Res. Lett.* **66,** 665–677 (1961).
5. Li, X. *et al.* Colorado Student Space Weather Experiment: differential flux measurements of energetic particles in a highly inclined low Earth orbit. *Geophys. Monogr. Ser.* **199,** 385–404 (2012).
6. Li, X. *et al.* First results from CSSWE CubeSat: characteristics of relativistic electrons in the near-Earth environment during the October 2012 magnetic storms. *J. Geophys. Res. Space Phys.* **118,** 6489–6499 (2013).
7. Li, X. *et al.* Upper limit on the inner radiation belt MeV electron intensity. *J. Geophys. Res. Space Phys.* **120,** 1215–1228 (2015).
8. Boscher, D., Bourdarie, S., Guild, T., O'Brein, P. & Heynderickx, D. International Radiation Belt Environment Modeling (IRBEM) library v.4.4, Toulouse, France (Panel on Radiation Belt Environment Modelling (PRBEM) Committee on Space Research (COSPAR), 2012).
9. Selesnick, R. S. *et al.* Inward diffusion and loss of radiation belt protons. *J. Geophys. Res. Space Phys.* **121,** 1969–1978 (2016).
10. Roederer, J. G., Hilton, H. H. & Schulz, M. Drift shell splitting by internal geomagnetic multipoles. *J. Geophys. Res.* **78,** 133–144 (1973).
11. Selesnick, R. S. & Blake, J. B. Relativistic electron drift shell splitting. *J. Geophys. Res.* **107** (A9), 1265 (2002).
12. Selesnick, R. S., Su, Y.-J. & Blake, J. B. Control of the innermost electron radiation belt by large-scale electric fields. *J. Geophys. Res. Space Phys.* **121,** 8417–8427 (2016).
13. Su, Y.-J., Selesnick, R. S. & Blake, J. B. Formation of the inner electron radiation belt by enhanced large-scale electric fields. *J. Geophys. Res. Space Phys.* **121,** 8508–8522 (2016).
14. Baker, D. N. *et al.* An extreme distortion of the Van Allen belt arising from the 'Halloween' solar storm in 2003. *Nature* **432,** 878–881 (2004).
15. Barker, A. B., Li, X. & Selesnick, R. S. Modeling the radiation belt electrons with radial diffusion driven by the solar wind. *Space Weather* **3,** S10003 (2005).
16. Li, X. *et al.* Modeling the deep penetration of outer belt electrons during the "Halloween" magnetic storm in 2003. *Space Weather* **7,** S02004 (2009).
17. Baker, D. N. *et al.* An impenetrable barrier to ultra-relativistic electrons in the Van Allen radiation belt. *Nature* **515,** 531–534 (2014).
18. Selesnick, R. S. Atmospheric scattering and decay of inner radiation belt electrons. *J. Geophys. Res.* **117,** A08218 (2012).
19. Selesnick, R. S. Stochastic simulation of inner radiation belt electron decay by atmospheric scattering. *J. Geophys. Res. Space Phys.* **121,** 1249–1262 (2016).
20. Sauvaud, J. A. *et al.* High energy electron detection onboard DEMETER: the IDP spectrometer, description and first results on the inner belt. *Planet. Space Sci.* **54,** 502–511 (2006).
21. Selesnick, R. S. High-energy radiation belt electrons from CRAND. *J. Geophys. Res. Space Phys.* **120,** 2912–2917 (2015).

Acknowledgements This work was supported in part by the National Science Foundation (NSF) CubeSat Program, NSF grant AGS 1443749, and NASA/Radiation Belt Storm Probes (RBSP)-Energetic particle, Composition and Thermal plasma (ECT) funding through Johns Hopkins University (JHU)/Applied Physics Laboratory (APL) contract 967399 under prime NASA contract NAS5-01072.

Author Contributions X.L. developed the project, directed the data analysis and was primarily responsible for writing the paper. R.S. was involved with the project from the beginning, gave advice on data analysis, and helped to revise the paper. Q.S. calibrated REPTile's response and produced related data and figures. K.Z. and H.Z. performed data analysis and produced related figures. D.N.B. gave advice on data analysis and revision of the paper. M.A.T. gave advice on data analysis and helped to revise the paper.

Author Information Reprints and permissions information is available at www.nature.com/reprints. The authors declare no competing financial interests. Readers are welcome to comment on the online version of the paper. Publisher's note: Springer Nature remains neutral with regard to jurisdictional claims in published maps and institutional affiliations. Correspondence and requests for materials should be addressed to X.L. (lix@lasp.colorado.edu).

Reviewer Information *Nature* thanks M. Hudson and the other anonymous reviewer(s) for their contribution to the peer review of this work.

© 2017 Macmillan Publishers Limited, part of Springer Nature. All rights reserved.

METHODS

Using measurements obtained from the REPTile experiment on board CubeSat, we convert the first channel's count rate to differential flux on the basis of the detector's response and the known energy spectrum of CRAND electrons (dashed line in Extended Data Fig. 2). REPTile's look direction is, for the vast majority of the time, close to 90° with respect to the magnetic field and thus measures locally mirroring particles. However, as the field of view of the instrument is large (±26°) and the passive attitude control allows the field of view to wobble by ±15° (see figure 3 of ref. 6), the measured particles can include non-local mirroring particles and can be a combination of trapped, quasi-trapped, and precipitating populations, depending on the spacecraft location.

The energy bandwidth of REPTile's first channel for this application is 0.48–1.63 MeV. The centroid given the quasi-trapped electron spectrum estimated from the CRAND β-decay spectrum is 0.49 MeV. The flux at a specific energy can be determined directly from the known β-decay spectrum and the well modelled instrument response[5,6,22]. We have chosen to calculate flux for 0.5-MeV electrons, owing to their closeness to the centroid and the convenience of the round number, and so as to compare our findings easily with those from other low-Earth-orbit instruments (such as DEMETER, which has an energy channel at 0.5 MeV).

By convolving the detector response (Extended Data Fig. 2, dotted line) with the quasi-trapped electron spectrum (solid line), which is given by equation (1), we can determine the differential electron flux at any energy. In Figs 1 and 3 we show the differential flux from neutron decay for the quasi-trapped electron population at 0.5 MeV. We note that the profiles of the quasi-trapped electrons are independent of the energy spectrum. Also plotted in Extended Data Fig. 2 is the normalized probability distribution of the kinetic energy of electrons generated by neutron decay (dashed line). We also used an exponential spectrum with $E_0 = 100$ keV (obtained from the expression $J \approx \exp(-E/E_0)$, where J is the ambient electron flux and E is the electron energy), based on DEMETER's measurements. We found that the difference between the flux values obtained from the exponential spectrum and those obtained from the CRAND energy spectrum for quasi-trapped electrons (Fig. 1) is within 10%.

Data availability. CSSWE data are publicly available at http://cdaweb.gsfc.nasa.gov. DEMETER data are publicly available at https://cdpp-archive.cnes.fr.

22. Schiller, Q., Mahendrakumar, A. & Li, X. REPTile: a miniaturized detector for a CubeSat mission to measure relativistic particles in near-Earth space. In *24th Annual AIAA/USU Conference on Small Satellites* SSC10-VIII-1 (2010).

© 2017 Macmillan Publishers Limited, part of Springer Nature. All rights reserved.

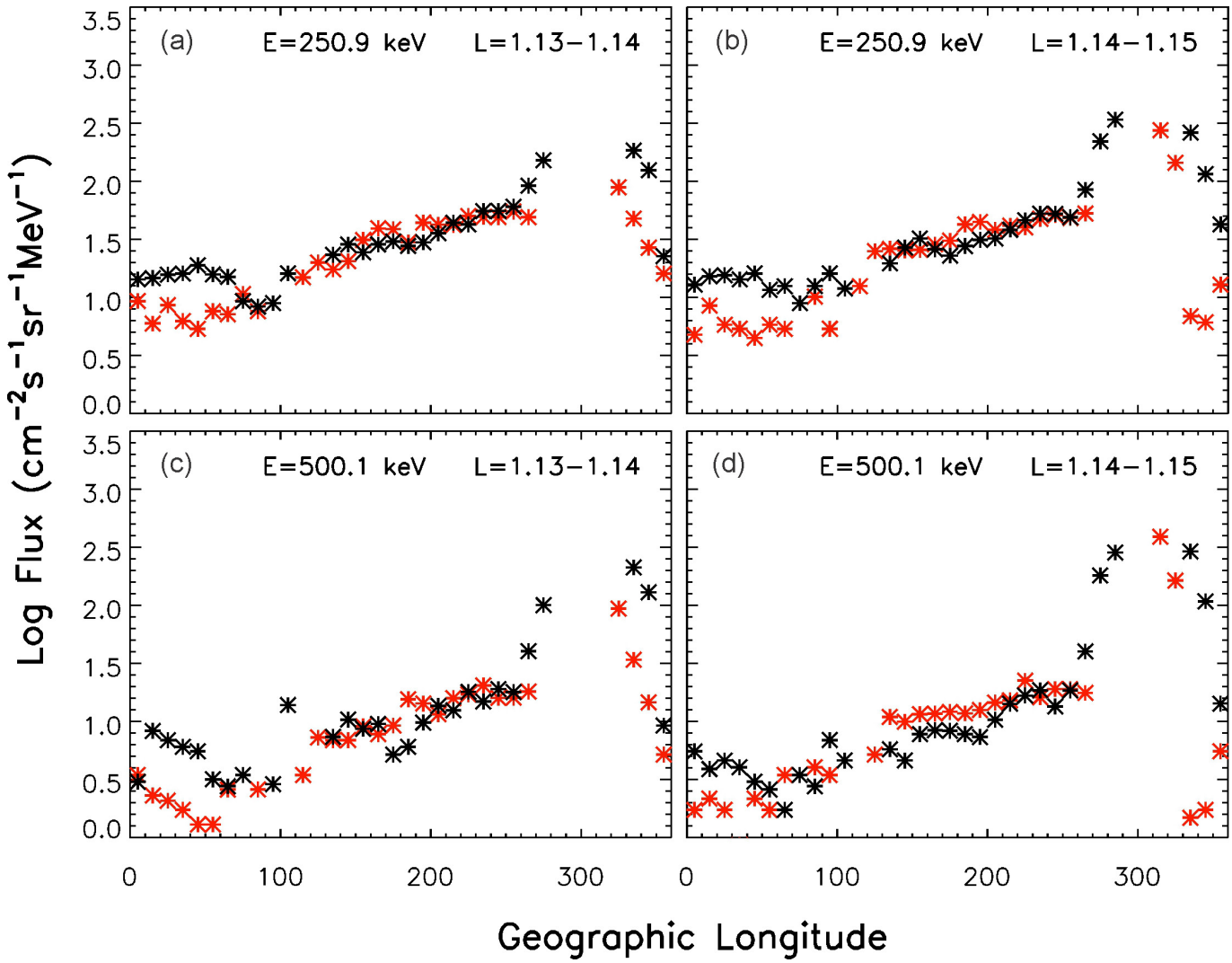

Extended Data Figure 1 | Confirmation of our findings from other satellite measurements. Electron flux measured by the DEMTER satellite[20], which has an altitude of 710 km and inclination of 98.3°, plotted versus geographic longitude for different energies (E) and different L bins, and averaged over every 10° for the time period 20–30 April 2010. The magnitude of flux of quasi-trapped electrons at 0.5 MeV is the same as that measured by REPTile.

© 2017 Macmillan Publishers Limited, part of Springer Nature. All rights reserved.

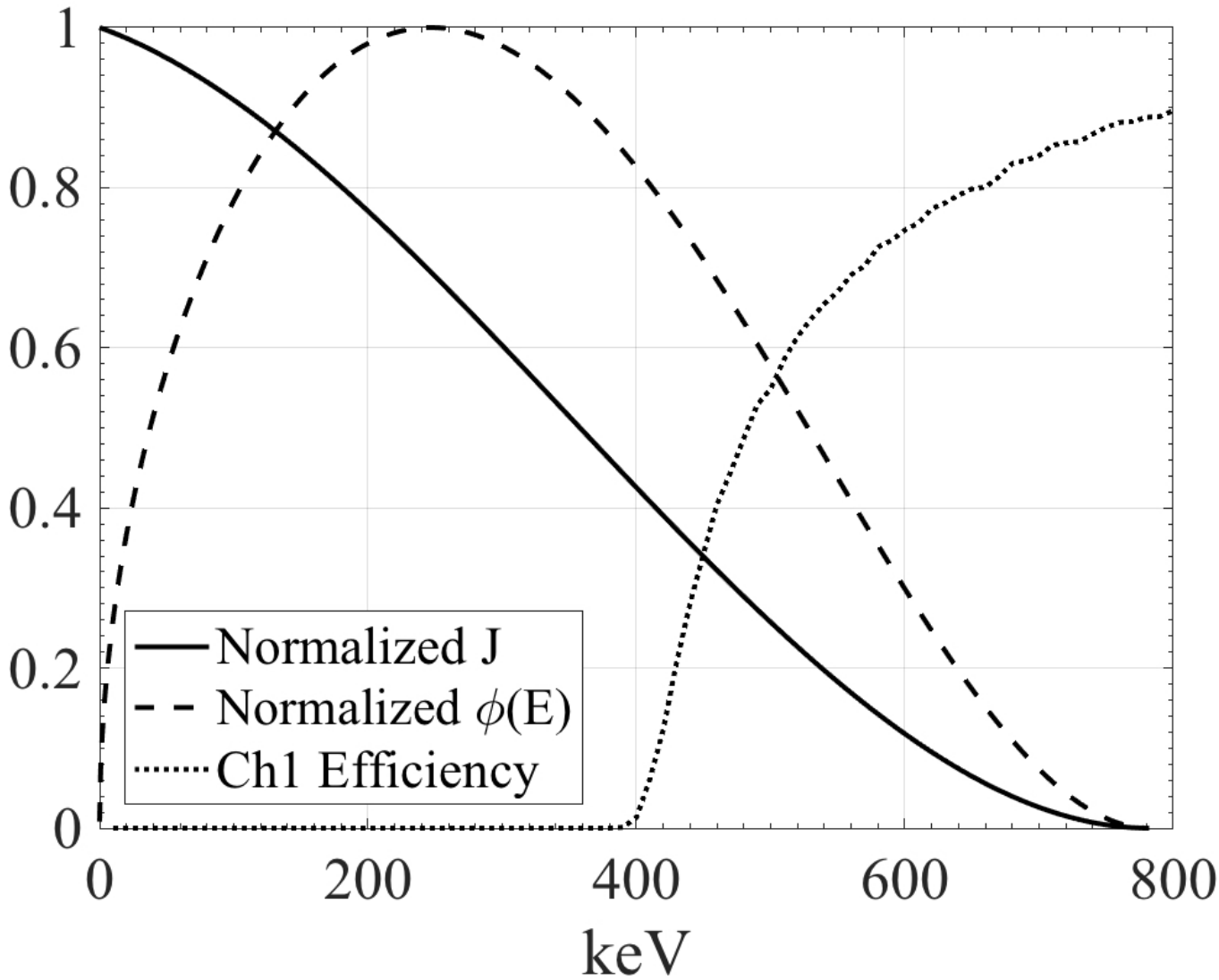

Extended Data Figure 2 | Flux conversion on the basis of the β-decay spectrum of albedo neutrons and the detector's energy response. The ambient electron flux (*J*; solid line) is normalized and calculated from equation (1). The dashed line, representing the known β-decay spectrum ($\varphi(E)$), is normalized to a maximum value of 1 (but the value of $\varphi = 1.2$ used in the text is normalized with the area under the curve that is equal to 1) and calculated using equation (4) of ref. 21). The response of REPTile channel 1 (Ch1) to normally incident electrons is shown by the dotted line. The *y* axis shows *J*, the normalized β-decay spectrum (maximum normalized to 1), and the channel 1 efficiency (maximum is 1).

© 2017 Macmillan Publishers Limited, part of Springer Nature. All rights reserved.